
**Universitat de les Illes Balears**

# Optical properties of 2D Majorana nanowires

Daniel Ruiz Reynés

**Master's Thesis**

Master's degree in Physics of Complex Systems

at the

UNIVERSITAT DE LES ILLES BALEARS

2013-2014

*Author:* _____

*August 20, 2014*

*Certified by:* _____

*Llorenç Serra Crespí*
*UIB Master Thesis Supervisor*

*Accepted by:* _____

*Raúl Toral Garcés*
*Director of the Master in Physics of Complex Systems*

# Agraïments

En primer lloc vull agrair al meu tutor, Llorenç Serra, tota l'ajuda que m'ha oferit i el que és més important, per despertar en jo l'interès per la Mecànica Quàntica, i fer-me gaudir d'aquesta branca de la Física. A en Javier Osca per la seva ajuda. Als Master Students per ser els meus companys de travessia. També vull agrair a la meva família el seu recolzament incondicional des de sempre i per soportar amb paciència les meves incessants explicacions. Finalment a na Neus i ella ja sap perquè.

# Contents

# Abstract

The main aim of the present work is to study the properties of the Majorana states in the context of condensed matter, and more specifically the optical properties of hybrid semi-superconductor nanowires. First we explain the most important concepts referent to the Majorana states. We address the importance for particle physics, for quantum computation and stress the results with more impact in the field. In second place, we introduce the necessary methods to describe Majorana states in two-dimensional systems. We introduce the Bogoliubov-deGennes hamiltonian, we study its properties and the most important results necessary to compute the optical properties. The third and final chapter is the novel contribution of this work. We present first the used theoretical formalism, after that we study the results of the optical spectrum changing different parameters, the dependence on magnetic field, the light polarization effects and the influence of temperature. This work gives guides for the experimental detection of Majorana states in semiconductor nanowires with optical spectroscopy.

# Chapter 1

# Introduction

Majorana states were suggested in 1937 by Ettore Majorana [1], who introduced in the context of theoretical physics the idea of fermionic particles that are at the same time their own antiparticles. These quantum states are particular solutions of the Dirac equation [2] that might appear under specific conditions. The Dirac equation describes relativistic quantum mechanics for spin-1/2 fermions and has complex solutions $\psi$ for the fermionic wave function at both positive and negative energies. A fundamental idea is the Dirac interpretation of the vacuum as a sea of infinite particles occupying all the negative-energy solutions which allowed him to predict the existence of the positron. If we think in the negative energy levels filled with electrons and we move an electron from negative energy to positive energy we will leave a hole in the sea with opposite charge. The idea is that the state with a hole in the negative-energy sea is a positively charged particle of ordinary positive energy [3]. Generalizing, each particle has an associated antiparticle with the same mass, the same spin but with an opposite charge and when the two are in the same quantum state they annihilate. An electron and a positron annihilate generating a photon. The reverse process is also possible; i.e., a photon can generate an electron-positron pair. Figure 1.1 shows a sketch of these processes.

The charge conjugation transformation $\psi \rightarrow \psi^*$ changes a positive energy state $\psi$ (representing a particle) into its associated negative-energy hole (representing the antiparticle). This implies that a particle described with state $\psi$ that is its own antiparticle must be represented by a real wave function. Majorana found a way of rewriting Dirac equation such that it becomes

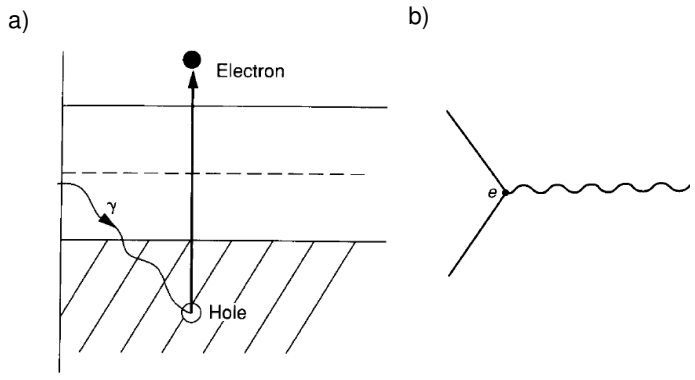


**Figure 1.1:** Sketch of an electron-positron pair process represented as a) a transition in the Dirac's sea of infinite negative energy states, b) a Feynman diagram. [3]

purely real, whose solutions must therefore be real. These real solutions are the Majorana states that are their own antiparticles. Even though in high-energy physics the measurement of a Majorana particle would be an important discovery, they have not been detected so far. Some particles like neutrinos [4] have been considered, but at the end neutrinos have not been good candidates.

In recent years in condensed matter physics the concept of Majorana states has attracted much attention, partly due to the connections with particle physics and partly due to the possible applications in quantum computation [5–9]. Condensed matter physics provides an alternative to the detection of Majorana fermions, although in this field Majorana modes present some differences with respect to the previous case. The main difference is that the state does not refer to a particle, but to a collective state that emerges due to many-body interactions, with the Bogoliubov-de Gennes hamiltonian determining the behavior of quasiparticles. In this scenario particles and antiparticles are associated to electrons and holes in the solid state system, both having a finite effective mass, the same spin and an opposite charge. The system has particle-hole symmetry, implying that for each state of energy $E$ there exist another state with opposite energy $-E$. These Majorana fermions, however, can not be realized in a raw material since superconductivity is needed to form Majorana modes. Superconductivity creates Cooper pairs, composed of two electrons that attract themselves due to effects of the lattice. The fact is that to promote a quasiparticle to a positive energy level an additional energy is needed to separate the electron pair, the manifestation of this is the presence of a gap in the energy spectrum. In a hybrid semiconductor-supercoductor nanowire a Majorana mode is formed when the lowest energy levels collapse to zero and the fermionic states fuse in a unique state characterized by a wave function localized on the nanowires tips.

In physics, quantum states can be classified in fermionic states and bosonic states. Fermionic states change sign of the wave function under interchange of particles, while bosonic states preserve sign under interchange of particles. Another type of states, called anyons, change by a global phase of the wave function (different to $\pm 1$) under interchange of particles. Finally, there are non-abelian anyons that change completely the wave function in a non-trivial way when two particles are interchanged. Majorana states are an example of non-abelian anyons and, for this reason, they are so important in quantum computation. The main goal of quantum computation is to encode and manipulate information using quantum states. For this reason the knowledge of transformation of quantum states is a valuable asset in this field. Non-abelian anyons become relevant in this sense, since exchanging them you can transform completely the state and its encoded information. Moreover, due to their localized character Majorana modes are topologically protected against decoherence, the energy gap protects them from sources of noise. It is believed that because of these features Majorana states are good proposals to be used in future to make quantum computers.

Experimental evidences of the existence of Majorana states already exist [10–14]. They report electrical measurements of a zero-bias conductance peak in the differential conductance. These measurements have been done in a indium antimonide (InSB) nanowires, connected with a gold contact and an superconducting electrode of niobium titanium nitride (NbTiN). However, the conductance peak is not enough to unambiguously confirm the existence of the Majorana states and more evidences are presently looked for.

The legacy of E. Majorana is nowadays an important topic in science. Its theoretical implications and its posible applications to new technologies justify the strong efforts devoted by the scientific community to understand this topic in more detail.

# Chapter 2

# A 2D model

The second chapter of this work is devoted to the description of Majorana states in a 2D model. We address the main properties of the system and the numerical implementation to describe them as well. In section 2.1 we introduce the Bogoliubov-deGennes hamiltonian and briefly describe the main characteristics of the formation of Majorana states. Section 2.2 explains particle-hole symmetry and the implications for the optical spectrum. The third part, section 2.3, presents the methodology to solve numerically the Bogoliubov-deGennes hamiltonian. Finally, section 2.4 shows the corresponding results, necessary for the optical-spectroscopy analysis of the third chapter.

## 2.1 The Bogoliubov-deGennes Hamiltonian

We model a semiconductor nanowire with spin-orbit Rashba coupling, in the presence of a magnetic field, while a nearby superconductor induces the superconductivity effect due to proximity. These kind of systems can be modeled using a 1D approach; however, in order to have a more accurate description we use a 2D model that reproduces in a more realistic way the system, still not hindered by time consuming calculations characteristic of a 3D model. Moreover, this second dimension will allow us to understand in the following chapter more properties of the system. Definitely the second dimension gives us more freedom in experiment than a purely 1D approach. One of the important reasons why these systems are often modeled in one dimension is because Majorana states are formed in narrow long systems, the unidimensional approach satisfying very well this condition. Nevertheless a strong confinement in one of the dimensions is needed to form Majorana modes in two dimensional systems.

The system is described by the Bogoliubov-deGennes Hamiltonian that can be expressed in terms of the kinetic energy, Zeeman, superconductivity and Rashba spin-orbit coupling as

$$\mathcal{H}_{BdG} = \left[\frac{p_x^2 + p_y^2}{2m} + V(x,y) - \mu\right]\tau_z + \Delta_B\,\vec{\sigma}\cdot\hat{n} + \Delta_0\,\tau_x + \frac{\alpha}{\hbar}(p_x\sigma_y - p_y\sigma_x)\tau_z\ . \tag{2.1}$$

From left to right the contributions to Eq. 2.1 are: kinetic energy with $\vec{p}$ and $m$ the momentum and the effective mass, respectively; $V(x,y)$ is an electric potential representing the shape of the nanowire; $\mu$ the chemical potential; $\vec{\sigma}$ and $\vec{\tau}$ are vector operators for spin and isospin (in electron-hole space) respectively; $\Delta_B$, $\Delta_0$ and $\alpha$ represent the Zeeman, superconductivity and Rashba coupling energies, respectively; finally, $\hat{n}$ is the direction of the magnetic field in the $xy$ plane, that can also be expressed in terms of the azimuthal angle $\phi$ as $\hat{n} \equiv (\cos\phi, \sin\phi)$. A sketch of the physical system is given in figure 2.1.

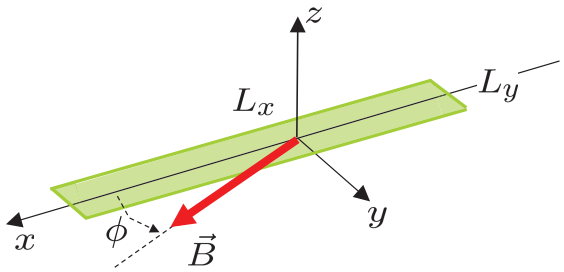


**Figure 2.1:** Sketch of the planar nanowire in a tilted magnetic field.

A natural unit system of the Bogoliubov-deGennes Hamiltonian can be determined by the coupling constants $\alpha$, the planck constant $\hbar$, and the effective mass $m$ of the electrons and holes in the semiconductor. The hamiltonian becomes dimensionless in the following unit system,

$$E_{so} = \frac{\alpha^2 m}{\hbar^2}, \quad L_{so} = \frac{\hbar^2}{\alpha m}, \quad T_{so} = \frac{\hbar^3}{\alpha^2 m}. \tag{2.2}$$

In these units the constants $\alpha$, $\hbar$, and $m$ are chosen equal to one. All the presented results in this chapter and the following one are given in this units, unless otherwise specified.

The superconductivity effect induces particle-hole symmetry, this yielding symmetric energy eigenvalues with respect to the chemical potential. Moreover, superconductivity is responsible for an energy gap around the chemical potential. The Rashba spin-orbit coupling comes from the interaction between the electron spin and its own motion. Finally the Zeeman term allows us to drive the system into different regimes. The Majorana state appears when the Zeeman term reaches a critical value. When the magnetic field is oriented in the long direction of the nanowire ($\phi = 0$) and magnetic field increases, the lowest positive eigenvalue with respect to the fermi level goes down. When the eigenvalue reaches zero energy the Majorana is formed, characterized by two maxima of the probability density localized in the edges of the nanowire. This transition, leading to the creation of Majorana modes is called in the literature a topological transition. The critical value for Zeeman energy is given by the following relation

$$\Delta_B^{(c)} = \sqrt{\Delta_0^2 + \mu^2}\,. \tag{2.3}$$

For $\Delta_B < \Delta_B^{(c)}$ there is no Majorana mode, while for $\Delta_B > \Delta_B^{(c)}$ a Majorana can appear. Equation (2.3) results from the analysis of a one dimensional semi-infinite system as explained in [15–17]. This approximation is valid for our two dimensional limit when the nanowire is thin enough. Although the fulfillment of Eq. (2.3) is a necessary condition to obtain a Majorana mode, it is not sufficient. For greater values of the magnetic field higher levels of energy go to zero as is shown in Ref. [16], this higher levels collapse with the existing Majorana mode producing the interaction between them due to effective repulsion, this breaking the Majorana zero-energy state. At the end, we only have a specific range of the Zeeman energy where Majorana modes may be present.

The reader must notice that we have not said anything about magnetic fields in other directions different from $\hat{x}$. The effects of tilting the magnetic field are discussed in Ref. [18] finding the so-called projection rule for a unidimensional nanowire. When the magnetic field is in tilted direction the range of Zeeman energies in which Majorana is possible is reduced. For magnetic fields in the $xy$ plane the Majorana mode delocalizes when the azimuthal angle $\phi$ exceeds a

critical value. If $\phi$ is fixed and $\Delta_B$ is increased, the projection rule yields a superior limit for $\Delta_B$ beyond which Majorana modes are not present. Moreover, if magnetic field is out of the $xy$ plane, the polar angle decreases from 90° and the formation of Majorana states is destroyed due to orbital effects. However, since we have not taken into account the orbital effects appearing when the magnetic field has non-zero component in the $\hat{z}$ axis, we will restrict to in-plane tilts in this work.

## 2.2 Particle-Hole symmetry

The main aim of this section is to provide an important result for the third chapter. For this reason we need to introduce particle-hole symmetry operator

$$\Theta\mathcal{H} = -\mathcal{H}\Theta, \tag{2.4}$$

where $\Theta$ is the time-reversal-plus-charge-conjugation operator (or time-charge inversion for short).

$$\Theta = -\sigma_y\tau_y\mathcal{K} = \begin{pmatrix} 0 & 0 & 0 & 1 \\ 0 & 0 & -1 & 0 \\ 0 & -1 & 0 & 0 \\ 1 & 0 & 0 & 0 \end{pmatrix}\mathcal{K} \tag{2.5}$$

and $\mathcal{K}$ is the conjugation operator.

A system with particle-hole symmetry fulfills that if $|\Psi_E\rangle$ is an eigenstate with energy $E$ then $\Theta|\Psi_E\rangle$ is an eigenstate with energy $-E$. Let

$$\mathcal{H}|\Psi_E\rangle = E|\Psi_E\rangle. \tag{2.6}$$

Applying the time-charge inversion operator to both sides,

$$\Theta\mathcal{H}|\Psi_E\rangle = E\Theta|\Psi_E\rangle \Rightarrow -\mathcal{H}\Theta|\Psi_E\rangle = E\Theta|\Psi_E\rangle \Rightarrow \mathcal{H}\left(\Theta|\Psi_E\rangle\right) = -E\left(\Theta|\Psi_E\rangle\right) \tag{2.7}$$

Then $|\Psi_{-E}\rangle = \Theta|\Psi_E\rangle$.

Now we want to prove an important property with Bogoliubov-deGennes eigenstates: the matrix element of the momentum operator with opposite states in energy is zero.

$$\begin{aligned} \langle\Psi_E|p_i|\Psi_{-E}\rangle &= \langle\Psi_E|p_i\Theta|\Psi_E\rangle = -i\hbar\int_{-\infty}^{+\infty}(\psi^*_{\uparrow\Uparrow},\psi^*_{\uparrow\Downarrow},\psi^*_{\downarrow\Uparrow},\psi^*_{\downarrow\Downarrow})\,\frac{\partial}{\partial x_i}\begin{pmatrix} \psi^*_{\downarrow\Downarrow} \\ -\psi^*_{\downarrow\Uparrow} \\ -\psi^*_{\uparrow\Downarrow} \\ \psi^*_{\uparrow\Uparrow} \end{pmatrix} dx_i \\ &= -i\hbar\int_{-\infty}^{+\infty}\frac{\partial}{\partial x_i}\left(\psi^*_{\uparrow\Uparrow}\psi^*_{\downarrow\Downarrow} - \psi^*_{\uparrow\Downarrow}\psi^*_{\downarrow\Uparrow}\right)dx_i = 0\,. \end{aligned} \tag{2.8}$$

Due to boundary conditions the integral is zero. This result is very important for the following chapter because this matrix element is involved in the transition from the state with energy $-E$ to the state with energy $E$. We can say now that these transitions will not contribute to the optical spectrum.

## 2.3 Numerical methods

We shall solve the Schrödinger equation with the above Hamiltonian,

$$\mathcal{H}_{BdG}\Psi(x,y,\eta_\sigma,\eta_\tau) = E\Psi(x,y,\eta_\sigma,\eta_\tau)\ , \tag{2.9}$$

expanding the wave function in $z$-basis spinors for spin and isospin, $\chi_{s_\sigma}$ and $\chi_{s_\tau}$,

$$\Psi(x,y,\eta_\sigma,\eta_\tau) = \sum_{s_\sigma,s_\tau} \psi_{s_\sigma,s_\tau}(x,y)\chi_{s_\sigma}(\eta_\sigma)\chi_{s_\tau}(\eta_\tau)\ . \tag{2.10}$$

The wave function variables are the space coordinates $(x,y) \in \Re$, the spin $\eta_\sigma \in \{\uparrow,\downarrow\}$ and isospin $\eta_\tau \in \{\Uparrow,\Downarrow\}$. The quantum numbers of spin and isospin are $s_\sigma = \pm$ and $s_\tau = \pm$ and it is fulfilled that

$$\vec{\sigma}\cdot\hat{n}\chi_{s_\sigma}(\eta_\sigma) = s_\sigma\chi_{s_\sigma}(\eta_\sigma)\ , \tag{2.11}$$

$$\tau_z\chi_{s_\tau}(\eta_\tau) = s_\tau\chi_{s_\tau}(\eta_\tau). \tag{2.12}$$

Projecting equation (2.1) on $\langle s_\sigma s_\tau|$ we find the following system of equations for the components $\psi_{s_\sigma,s_\tau}(x,y)$ of the wave function.

$$\begin{aligned}\left[\left(\frac{p_x^2+p_y^2}{2m}+V(x,y)-\mu\right)s_\tau - E\right]\psi_{s_\sigma s_\tau}(x,y) \quad &+ \quad \Delta_B(\cos\phi - is_\sigma\sin\phi)\,\psi_{\bar{s}_\sigma s_\tau}(x,y) \\ +\Delta_0\,\psi_{s_\sigma\bar{s}_\tau}(x,y) \quad &- \quad \frac{\alpha}{\hbar}s_\tau(is_\sigma p_x + p_y)\,\psi_{\bar{s}_\sigma s_\tau}(x,y) = 0\ ,\end{aligned} \tag{2.13}$$

where we use the notation $\bar{s} = -s$. In order to solve this equation system with partial derivatives we use numerical techniques. We have discretized the space in a square lattice, where $N_x$ and $N_y$ are the number of points of each dimension. The boundary conditions is simply vanishing of the wave function at the edges of the grid. We use finite differences to describe the partial derivatives, then we have a component of the wave function at each position of the lattice. This discretization of the wave function in space allows us to construct a system of equations for all this components that can be expressed in matrix form.

The size of the matrix is $\mathcal{N}\times\mathcal{N}$, where $\mathcal{N} = 4N_xN_y$, the factor four coming from the 4 components of the wave function. Once we have this matrix, to find the solution we have to diagonalize it. One useful property of this matrix is that many of its elements are zero, i.e., it is highly sparse. The diagonalization problem is solved using a diagonalization subroutine for sparse matrices [19] that yields the eigenvalues lying near a given reference value. It is important to realize that for $N_x = N_y = 100$ it is $\mathcal{N} = 40000$, and one diagonalization is highly time consuming with non-sparse routines. For this reason it is important to avoid all unnecessary computations with zero-valued matrix elements. The wave function will be confined in the region of the nanowire imposed by the potential, many points of the lattice out of this region can be avoided because the wave function will be extremely small. Finally, when we have the solution we can compute the quantities that we need like the probability density of a given eigenstate, or the variation of the eigenvalue spectrum with different parameters.

The last we mention in this section on numerical methods is how we model the shape of the nanowire. We model a nanowire of size in the order of $\mu$m, that is, much higher than the atomic scale. This allows us to use a smooth potential. We construct square shape potential such that each side of the square is modeled using a two dimensional fermi function

$$f(x,y) = \left[1+\exp\left(\frac{(y-y_0)\cos\theta-(x-x_0)\sin\theta-L}{s}\right)\right]^{-1}\ , \tag{2.14}$$

where the softness degree is controlled by parameter $s$ and the limit line where the function changes from 0 to 1 is

$$y = y_0 + (x - x_0)\tan\theta - \frac{L}{\cos\theta}\ . \tag{2.15}$$

The functional form Eq. (2.14) conveniently models different borders of the nanowire changing the parameters $x_0$, $y_0$, $L$ and $\theta$. The parameters $x_0$, $y_0$ are the central position of the nanowire, $L$ is the distance of the line to the center and $\theta$ is the angle that form this line respect to the $x$-axis.

## 2.4 Results

In this section we are going to present the numerical solutions of the above hamiltonian. This numerical solution correspond to the following set of parameters: We use a spatial dimension from $x_{min} = -15L_{so}$ to $x_{max} = 15L_{so}$ and the same for $y$, 101 points for the discretization in space in both directions. The shape of the nanowire is a rectangle of $L_x = 25L_{so}$ and $L_y = 2L_{so}$, a rather thin nanowire. The maximum value of the potential, out of the nanowire, is $V_0 = 5E_{so}$ and the softness of the fermi functions $s = 0.1$, these two values mimic a square well potential but with a little softness that is necessary for the numerical resolution.

We have taken the superconductivity energy $\Delta_0 = 0.25E_{so}$ that allows us to find Majorana state for a given Zeeman energy and, for simplicity, the chemical potential has been put equal to zero $\mu = 0$. Finally the magnetic field is taken in $x$ direction $\phi_B = 0$. We vary the Zeeman energy in order to see the emergence of the zero modes. We want to emphasize that this set of parameters will be used in all the rest of the work. We have made this choice for one reason, we want a representative set of parameters showing Majorana states for a good range of magnetic fields. There are more sets of parameters that fulfill this condition and that could be used to do the same analysis. For example, another $L_x/L_y$ ratio for a thinner or wider potentials, or another chemical potential $\mu$. In this work our purpose is giving an example of a good configuration presenting clear Majorana modes.

Next we present the evolution of the eigenvalues of the system as a function of the magnetic field in Fig. 2.2. We only display the 8 eigenvalues lying closer to zero energy, to avoid excessive computational times. We present also in the same graph the probability density of the lowest positive eigenvalue for selected cases in order to see how the system evolves with increasing Zeeman energies. For very low $\Delta_B$'s all the eigenvalues are nearly degenerate at two energies and the probability density is similar to that of a square well potential. When the Zeeman energy increases, the energy levels start to split, the gap becoming smaller and the first eigenfunction shows a quenched probability in the middle of the nanowire. For $\Delta_B \approx 0.42E_{so}$ the gap closes completely and the Majorana forms, this fact can be appreciated because the wave function is characterized by two probability maxima well localized on the edges of the nanowire. If we continue increasing the Zeeman energy the gap reopens, but one state remains 'trapped' in the middle of the gap, the Majorana state.

The gap with the Majorana state in the middle effectively protects the Majorana state from decoherence due to noise and disorder. If we focus on the probability density, increasing the magnetic field the localized maxima spread on the nanowire more and more until the second transversal mode goes to zero to form a second Majorana. However mode-mode interactions prevent the formation of these states and we can see a qualitative change of behaviour in the probability density.

We can see in more detail the probability densities for three different Zeeman energies in figure 2.3. The figure displays the probabilities for representative values of Zeeman parameter,

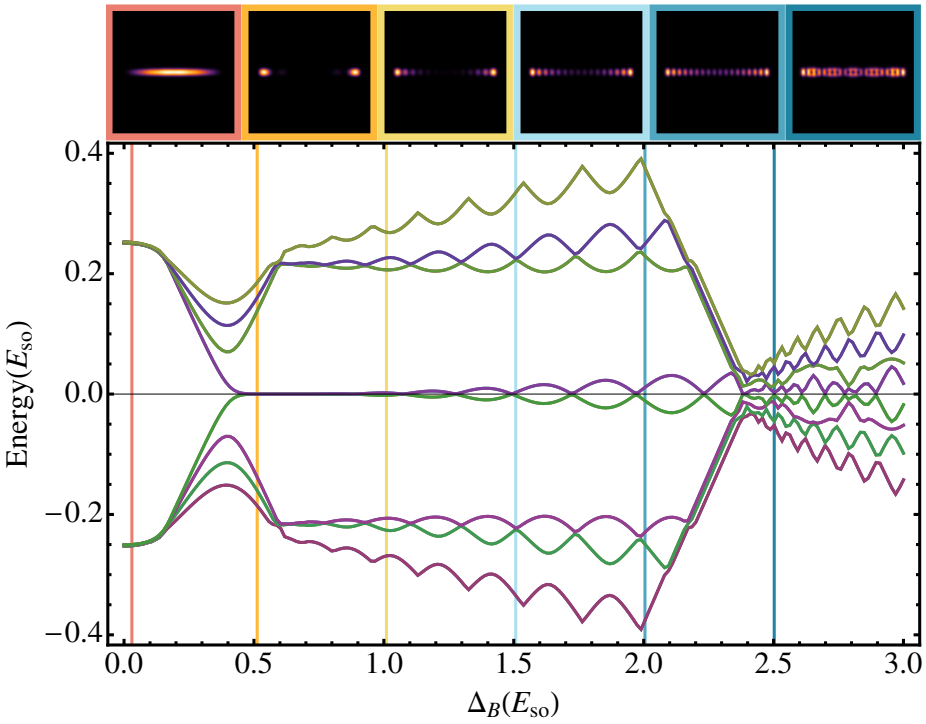


**Figure 2.2:** Representation of the eight eigenvalues lying closer to zero energy as a function of Zeeman energy $\Delta_B$. We present also six different cuts (vertical lines) corresponding to different $\Delta_B$'s, showing the probability density of the lowest positive eigenvalue at the corresponding Zeeman energy. The color of each line and frame are matched to better indicate the value of $\Delta_B$ for each density.

before the Majorana, on the Majorana and much after the Majorana formation.
We have now all that we need to study the optical properties of the system in Chap. 3, the energy eigenvalues and the eigenfunctions. We will not need to increase the Zeeman energy much beyond $\Delta_B = 0.5E_{so}$, because we only intend to analyze the formation of the Majorana state. One thing that we will have to increase is the number of eigenvalues in order to study the convergence with the number of transitions.

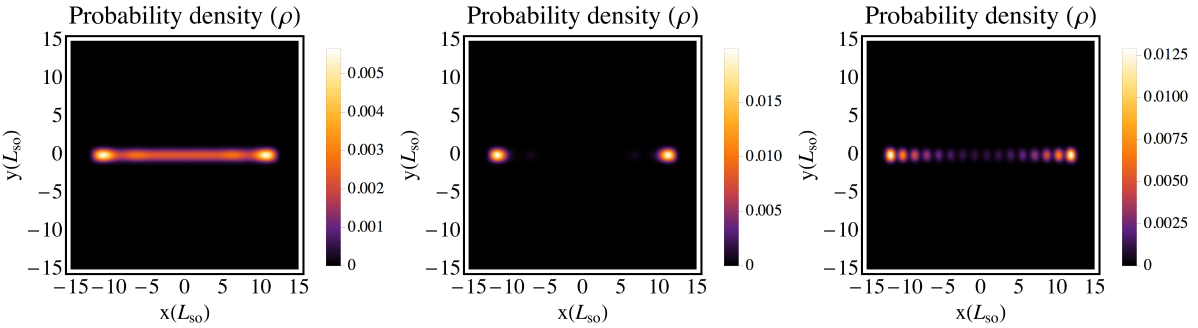


**Figure 2.3:** Probability densities for three selected Zeeman energies $\Delta_B = 0.392$, 0.588, 1.492 $E_{so}$ respectively. The first plot is before the formation of the Majorana state. The second corresponds to when the Majorana state is well formed and presents two maxima on the edges of the nanowire. Finally, the third is passed the range of the Majorana state when the edge modes delocalize.

# Chapter 3

# Spectroscopy

The third chapter of the Master Thesis is devoted to the calculation of the optical properties of the system that we have discussed before. Our main interest is to find a clear manifestation of the presence of the Majorana state in the nanowire. The chapter is divided into two sections. Section 3.1 presents our formalism to compute the cross section and the numerical methodology. In section 3.2 we present the main results of our work, focusing on the dependence of the cross section on different physical quantities.

## 3.1 Theoretical Formalism

### 3.1.1 Time-Dependent Perturbation theory

First we are going to obtain the transition probability between two states for a given time-dependent potential. We will not use the natural units in the first part of this chapter in order to give more general expressions. However, at the end of the section on formalism we will come back to the natural units. The following formalism is explained in more detail in chapter 19 of Merzbacher's book [20]. The total hamiltonian of the system is decomposed into two terms, the Bogoliubov-deGennes hamiltonian $\mathcal{H}_{BdG}$ that corresponds to the unperturbed system and whose solutions are known, and the second term $V$ that corresponds to a small perturbation that depends on time. We do not specify yet that this potential corresponds to the electromagnetic field but for now it may represent a general potential,

$$\mathcal{H} = \mathcal{H}_{BdG} + V \ . \tag{3.1}$$

It will be useful to work in the interaction picture, starting from the Schrödinger equation,

$$i\hbar \frac{d|\Psi(t)\rangle}{dt} = (\mathcal{H}_{BdG} + V)|\Psi(t)\rangle \ , \tag{3.2}$$

that can be transformed with the time-dependent unitary operator,

$$i\hbar \frac{d|\tilde{\Psi}(t)\rangle}{dt} = \tilde{V}(t)|\tilde{\Psi}(t)\rangle, \tag{3.3}$$

where the wave function and the potential in the interaction picture read

$$|\tilde{\Psi}(t)\rangle = e^{\frac{i}{\hbar}\mathcal{H}_{BdG}t}|\Psi(t)\rangle, \quad \tilde{V}(t) = e^{\frac{i}{\hbar}\mathcal{H}_{BdG}t} V e^{-\frac{i}{\hbar}\mathcal{H}_{BdG}t}. \tag{3.4}$$

Next we can introduce the time evolution operator $\tilde{T}(t,t_0)$, that gives the evolution of $|\tilde{\Psi}(t)\rangle$

$$|\tilde{\Psi}(t)\rangle = \tilde{T}(t,t_0)|\tilde{\Psi}(t_0)\rangle, \tag{3.5}$$

where

$$\tilde{T}(t,t_0) = \mathcal{T}\exp\left[-\frac{i}{\hbar}\int_{t_0}^{t}\tilde{V}(t')dt'\right] \tag{3.6}$$

and $\mathcal{T}$ is the time ordering instruction.

The time dependent potential $V$ is a small perturbation, a weak external forcing that will not change the states in which the system can be asymptotically, only its occupation probabilities. This potential induces changes in the system from an eigenstate $|s\rangle$ to an eigenstate $|k\rangle$ (or a combination of them). Both the initial and final states are general solutions of the Bogoliubov-deGennes hamiltonian. We are interested in the probability to be in state $|k\rangle$ at time $t$ with $|s\rangle$ as initial state, specifically

$$\langle k|\tilde{\Psi}(t)\rangle = \langle k|\tilde{T}(t,t_0)|s\rangle\ . \tag{3.7}$$

At this step we must use perturbation methods to obtain a practical result. We use the following expression for the time evolution operator at first-order

$$\tilde{T}(t,t_0) = 1 - \frac{i}{\hbar}\int_{t_0}^{t}\tilde{V}(t')dt' + ...\ . \tag{3.8}$$

Using eq. 3.4 and the difference in energy $\hbar\omega_{ks} = E_k - E_s$ we can obtain the transition amplitude

$$\langle k|\tilde{T}(t,t_0)|s\rangle = \delta_{ks} - \frac{i}{\hbar}\int_{t_0}^{t}\langle k|V(t')|s\rangle e^{i\omega_{ks}t'}dt'. \tag{3.9}$$

The probability of the transition from $|s\rangle$ to $|k\rangle$ at time $t$ when $k \neq s$ is

$$P_{k\leftarrow s} = \left|-\frac{i}{\hbar}\int_{t_0}^{t}V_{ks}e^{i\omega_{ks}t'}dt'\right|^2. \tag{3.10}$$

This approximation is valid when the transition probabilities are small compared with one, for short time intervals between $t_0$ and $t$. However, with a transient perturbation that is weak enough the approximation becomes valid for all times, when the initial time goes to $-\infty$ and the final time to $+\infty$

$$\boxed{P_{k\leftarrow s} = \left|-\frac{i}{\hbar}\int_{-\infty}^{+\infty}V_{ks}e^{i\omega_{ks}t'}dt'\right|^2.} \tag{3.11}$$

### 3.1.2 Electromagnetic field perturbation

Now we are going to consider the action of light on the system, particularizing the general theoretical formalism of the previous part. We are going to obtain the induced perturbation due to the presence of incident electromagnetic radiation. We start with the hamiltonian of an atomic electron in the presence of an electromagnetic field

$$\mathcal{H} = \frac{1}{2m}\left(\vec{p} + \frac{e}{c}\vec{A}\right)^2 - e\phi\ . \tag{3.12}$$

Explicitly expanding the first term we have

$$\mathcal{H} = \frac{-\hbar^2}{2m}\nabla^2 - e\phi(\vec{r},t) + \frac{e}{mc}\vec{A}(\vec{r},t)\cdot\frac{\hbar}{i}\nabla - \frac{ie\hbar}{2mc}\left[\nabla\cdot\vec{A}(\vec{r},t)\right] + \frac{e^2}{2mc^2}\left[\vec{A}(\vec{r},t)\right]^2\ . \tag{3.13}$$

We will work in such conditions that the last term can be neglected. Moreover, choosing a suitable gauge the vector potential is sufficient to describe the pure radiation field. The so-called Coulomb gauge fulfills

$$\nabla^2\vec{A} - \frac{1}{c^2}\frac{\partial^2\vec{A}}{\partial t^2} = 0, \quad \phi = 0, \quad \nabla\cdot\vec{A} = 0. \tag{3.14}$$

With the above assumptions only the kinetic term and the third term of 3.13 remain for the perturbation due to pure radiation that we were looking for. Now we have the needed perturbation in terms of the vector potential and the momentum operator

$$V = \frac{e}{mc}\vec{A}\cdot\vec{p};. \tag{3.15}$$

For our purposes it is necessary to assume a superposition of plane waves as incident radiation, the corresponding vector potential being a wave packet. That is nothing more than a superposition of harmonic plane waves that propagate at the speed of light $c$ in direction $\hat{n}$ with polarization $\hat{e}$

$$\vec{A}(\vec{r},t) = \int_{-\infty}^{+\infty} A(\omega)e^{-i\omega(t-\frac{\hat{n}\cdot\vec{r}}{c})}\,\hat{e}\,d\omega\ . \tag{3.16}$$

The frequency amplitude $A(\omega)$ is a real function satisfying $A(\omega)^* = A(-\omega)$. Furthermore $\nabla\cdot A(\vec{r},t) = 0$ that implies $\hat{n}\cdot\vec{A}(\omega) = A(\omega)\hat{n}\cdot\hat{e} = 0$, i.e., polarization is orthogonal to the propagation direction. Inserting 3.16 in 3.15 we obtain the potential $V$ in the desired final form

$$\boxed{V = \frac{e}{mc}\int_{-\infty}^{+\infty} A(\omega)\,e^{-i\omega(t-\frac{\hat{n}\cdot\vec{r}}{c})}\,\hat{e}\cdot\vec{p}\,d\omega\ .} \tag{3.17}$$

### 3.1.3 Cross Section

Having the potential $V$ we can compute now the transition probability. The transition amplitude reads

$$\begin{aligned}
\langle k|\tilde{T}(+\infty,-\infty)|s\rangle &= -\frac{ie}{\hbar mc}\int_{-\infty}^{+\infty}\int_{-\infty}^{+\infty}\langle k|e^{i\frac{\omega}{c}\hat{n}\cdot\vec{r}}\vec{p}\cdot\hat{e}|s\rangle A(\omega)\,e^{i(\omega_{ks}-\omega)t'}\,d\omega dt' \\
&= -\frac{2\pi ie}{\hbar mc}\int_{-\infty}^{+\infty}\langle k|e^{i\frac{\omega}{c}\hat{n}\cdot\vec{r}}\vec{p}\cdot\hat{e}|s\rangle A(\omega)\,\delta(\omega_{ks}-\omega)\,d\omega \\
&= -\frac{2\pi ie}{\hbar mc}\,\langle k|e^{i\frac{\omega_{ks}}{c}\hat{n}\cdot\vec{r}}\vec{p}\cdot\hat{e}|s\rangle\,A(\omega_{ks})\ ,
\end{aligned} \tag{3.18}$$

and the corresponding transition probability, given by the modulus square of the transition amplitude,

$$P_{k\leftarrow s} = \frac{4\pi^2e^2}{\hbar^2m^2c^2}\,|A(\omega_{ks})|^2\,\left|\langle k|e^{i\omega_{ks}\frac{\hat{n}\cdot\vec{r}}{c}}\vec{p}\cdot\hat{e}|s\rangle\right|^2. \tag{3.19}$$

The quantity $|A(\omega)|^2$ can be related to the energy flux using the Poynting vector

$$\vec{\mathcal{N}} = \frac{c}{4\pi}\vec{\mathcal{E}}\times\vec{B}. \tag{3.20}$$

The following relation, proved in [20], allows us to derive the relation 3.22,

$$\int_{-\infty}^{+\infty}\vec{\mathcal{N}}\cdot\hat{n}dt = \int_0^{+\infty}\mathcal{N}(\omega)d\omega = \frac{1}{c}\int_0^{+\infty}\omega^2|A(\omega)|^2d\omega, \tag{3.21}$$

$$\mathcal{N}(\omega) = \frac{\omega^2}{c}|A(\omega)|^2. \tag{3.22}$$

The average energy transfer at frequency $\omega_{ks}$ is

$$\hbar\omega_{ks}P_{k\leftarrow s} = \frac{4\pi^2\alpha}{m^2\omega_{ks}}\left|\langle k|e^{i\omega_{ks}\frac{\hat{n}\cdot\vec{r}}{c}}\vec{p}\cdot\hat{e}|s\rangle\right|^2\mathcal{N}(\omega_{ks})\ , \tag{3.23}$$

where $\alpha = \frac{e^2}{\hbar c}$ is the fine structure constant.

The cross section is a fictitious area that placed perpendicularly to the electromagnetic radiation would be crossed by the same energy that the system absorbs. The absorbed energy in the interval $(\omega, \omega + d\omega)$ is

$$\sigma(\omega)\mathcal{N}(\omega)d\omega\ . \tag{3.24}$$

Then, the energy transfer at $\omega_{ks}$ is equal to the integral of this quantity in the neighborhood $\Delta\omega$ of the frequency $\omega_{ks}$

$$\int_{\Delta\omega}\sigma(\omega)\mathcal{N}(\omega)d\omega = \frac{4\pi^2\alpha}{m^2\omega_{ks}}\left|\langle k|e^{i\omega_{ks}\frac{\hat{n}\cdot\vec{r}}{c}}\vec{p}\cdot\hat{e}|s\rangle\right|^2\mathcal{N}(\omega_{ks}). \tag{3.25}$$

For now we are assuming only one transition, meaning that the cross section will have a narrow peak at $\omega = \omega_{ks}$, and we can do the following approximation,

$$\int_{\Delta\omega}\sigma(\omega)\mathcal{N}(\omega)d\omega \approx \mathcal{N}(\omega_{ks})\int_{\Delta\omega}\sigma(\omega)d\omega\ . \tag{3.26}$$

The integrated cross section is thus written in terms of the matrix element that involves the transition $s \to k$,

$$\int_{\Delta\omega}\sigma(\omega)d\omega = \frac{4\pi^2\alpha}{m^2\omega_{ks}}\left|\langle k|e^{i\omega_{ks}\frac{\hat{n}\cdot\vec{r}}{c}}\vec{p}\cdot\hat{e}|s\rangle\right|^2\ . \tag{3.27}$$

In an equivalent way, the peak of the cross section is nothing more than a Dirac delta with the appropriate amplitude,

$$\sigma(\omega) = \frac{4\pi^2\alpha}{m^2\omega_{ks}}\left|\langle k|e^{i\omega_{ks}\frac{\hat{n}\cdot\vec{r}}{c}}\vec{p}\cdot\hat{e}|s\rangle\right|^2\delta(\omega-\omega_{ks}). \tag{3.28}$$

Summarizing, we have obtained after some approximations the cross section for a transition from $s$ to $k$. However, in reality as we have seen in the previous chapter, there are more energy states than two. We will consider the complete spectrum as a superposition of the cross sections of all possible transitions at different energies. We must also take into account that with fermions not all transitions are physically allowed, as only occupied-unoccupied transitions are permitted. Considering the level occupations of the system we must introduce the Fermi occupation distributions. The probability of the state $|s\rangle$ being occupied is $f_s$, the probability of the state $|k\rangle$ being empty is $1 - f_k$ and the product is associated with the probability of the transition $s \to k$. We see how the occupation of the levels plays a role in figure 3.1 for a given temperature. Finally, the total cross section in natural units is

$$\boxed{\sigma(\omega) = 4\pi^2\alpha\sum_{k,s}\frac{1}{\omega_{ks}}\left|\langle k|e^{i\frac{\omega_{ks}}{c_{so}}\hat{n}\cdot\vec{r}}\vec{p}\cdot\hat{e}|s\rangle\right|^2\delta(\omega-\omega_{ks})\,f_s\,(1-f_k)\ .} \tag{3.29}$$

where $c_{so}$ is the speed of light in natural units.

As we can see from equation (3.29), the cross section explicitly depends on frequency $\omega$, light propagation direction $\hat{n}$ and polarization $\hat{e}$. It also has a temperature dependence that is hidden in the fermi functions. We will study the dependence of the cross section with all these variables in the following section. However, we argue now that the propagation direction $\hat{n}$ does not really influence the cross section, as a consequence of our system being in the dipolar approximation regime. The energy differences in our system are in the range $\hbar\omega_{ks} \approx 1E_{so} \approx 0.4$ meV for an InAs semiconductor. Then the associated wave length is $\lambda = 2\pi c/\omega_{ks} \approx 3$ mm while the maximum dimension of the nanostructure is of the order of the $\mu$m. The wave length of the light is thus typically much larger than the nanowire and, therefore, the electromagnetic radiation affects homogeneously all the nanostructure. It can be understood performing the expansion of the harmonic term,

$$e^{i\frac{\omega_{ks}}{c_{so}}\hat{n}\cdot\vec{r}} = 1 + i\frac{\omega_{ks}}{c_{so}}\hat{n}\cdot\vec{r} + \dots . \tag{3.30}$$

The second term of the expansion is three orders of magnitude smaller than one, allowing the replacement $e^{i\frac{\omega_{ks}}{c_{so}}\hat{n}\cdot\vec{r}} \approx 1$. This is the limit of the dipole approximation and it is for this reason that the propagation direction does not have any effect on the spectrum.

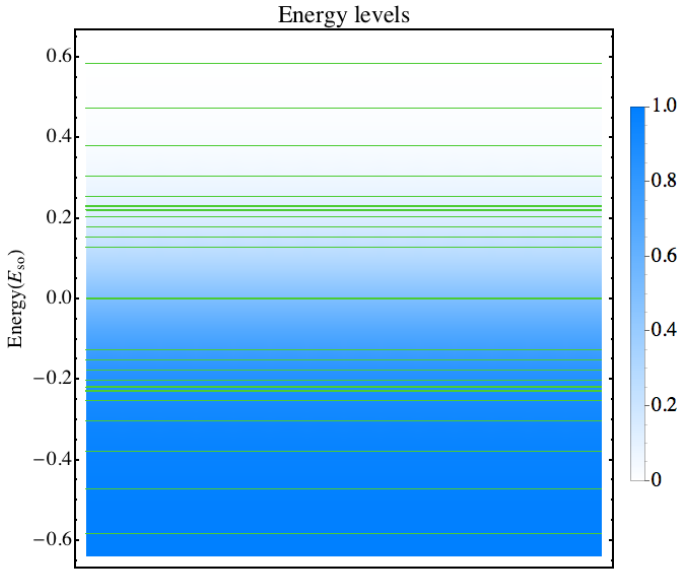


**Figure 3.1:** Energy spectrum for our system with Zeeman energy $\Delta_B = 0.5E_{so}$. The energy levels are represented by the horizontal (green) lines while the shading (colour) plot corresponds to the occupations as given by the Fermi distribution. It can be easily seen that for a temperature $T = 0.5$ K the Fermi sea smooth variations affect many levels close to zero energy.

The numerical computation of equation 3.29 requires considering all possible combinations of different transitions and computing the corresponding cross section matrix element for each one of them. For this we need to know all the energy levels and their respective wave functions, obtained in the previous chapter. Once we have the wave functions and the energy levels the most complicated thing is computing the matrix elements. The matrix elements involve a sum of the spatial integrals of the four components of the wave function. Moreover, the momentum operator involves also derivatives obtained with finite differences. The polarization direction $\hat{e}$ determines which component of the momentum operator is contributing. We characterize the

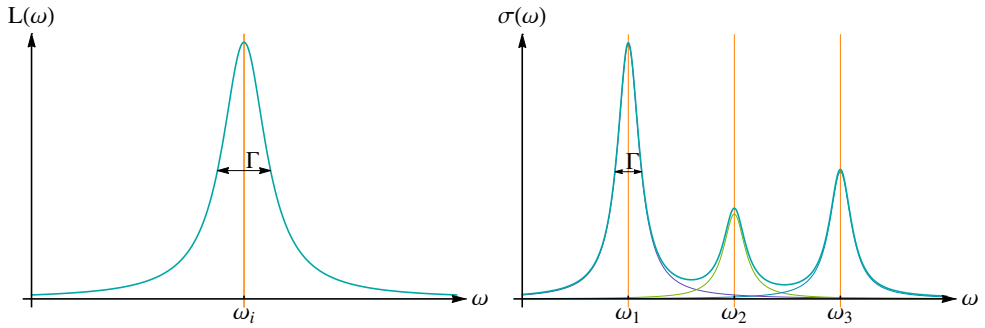


**Figure 3.2:** Transformation of a delta peak into a smoothed cross section using Lorentzians of width Γ. The left part corresponds to a single peak and the right one to multiple peaks of different heights. The central position of each peak is indicated by the vertical lines.

polarization with the azimuthal angle $\varphi$, varying from $\hat{x}$ for $\varphi = 0°$ to $\hat{y}$ for $\varphi = 90°$. The final result is a set of the possible frequencies and the respective values of the cross section.

Although we know how to compute the cross section as a collection of delta peaks, the results presented below are not the plain data. In order to give more physically intuitive plots we have used a normalized Lorentzian function for each peak

$$L(\omega) = \frac{1}{2\pi} \frac{\Gamma}{(\omega - \omega_i)^2 + \frac{\Gamma^2}{4}} , \tag{3.31}$$

where Γ is the width of the Lorentzian and $\omega_i$ its central position. The final cross section is a superposition of the Lorentzians for all the transitions,

$$\sigma(\omega) = \sum_i \frac{\sigma_i}{2\pi} \frac{\Gamma}{(\omega - \omega_i)^2 + \frac{\Gamma^2}{4}} , \tag{3.32}$$

where $\sigma_i$ and $\omega_i$ are the value of the cross section and the frequency of each transition, respectively. This is nothing more than a visualization technique to show the results in a more realistic way. We have taken the constant $\Gamma = 0.05 E_{so}$, a value that is useful to distinguish the contributions of the different transitions while, at the same time, it is in reasonable agreement with the experimental capabilities of measurement. With an InAs semiconductor $E_{so} = 0.4$ meV would correspond to an experimental resolution of 20 $\mu$eV, or what is the same 0.2 cm$^{-1}$. The equivalent resolution presented in our theoretical results is below the experimental resolution found in the bibliography [21–26], however it does not differ in a high magnitude. There are experiments with better resolutions but they are not focused on nanostructures [27].

The numerical implementation has been done in fortran to compute the results and with Mathematica for the graphical presentations. Specifically, the part of the code corresponding to the cross section calculations does not present a high computational cost. As mentioned in the previous chapter the resolution of the hamiltonian eigenvalue problem is the most demanding part.

## 3.2 Results

This section contains the main results of this master thesis. Here we discuss the electromagnetic cross section of 2D Majorana nanowires focussing, specifically, on the elucidation of the signatures of the presence of zero modes. Thus, our main goal is to provide guides for the detection of zero modes with optical spectroscopy.

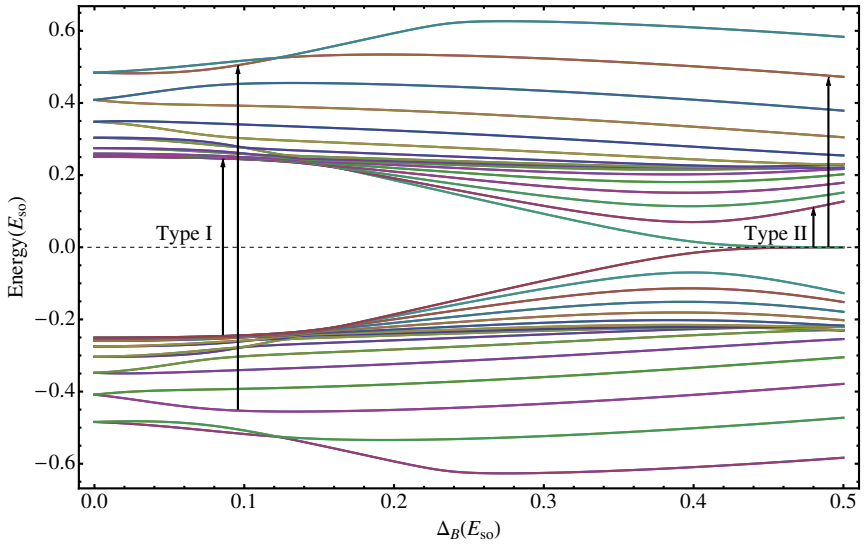


**Figure 3.3:** Evolution with $\Delta_B$ of the set of 32 energy eigenvalues lying closer to zero energy. Notice how the zero-energy mode appears for $\Delta_B > 0.42E_{so}$.

### 3.2.1 Magnetic field dependence

The first results that we want to present are the dependence of the spectrum of eigenvalues on the Zeeman energy. This dependence explicitly shows the appearance of a Majorana state when $\Delta_B$ increases and, for this reason, it is important to understand how magnetic field affects the spectrum. In a finite nanowire the topological transition from absence to presence of a zero mode occurs in a smooth way. This transition becomes sharp only in the semi infinite system, where a zero mode requires

$$\Delta_B > \sqrt{\Delta_0^2 + (\mu - \varepsilon_n)^2}\,, \tag{3.33}$$

with $\varepsilon_n = \hbar^2\pi^2 n^2/(2mL_y^2)$ $(n = 1, 2, \ldots)$ the transverse mode energies depending on the transverse length $L_y$.

As we are mainly interested in the formation of a Majorana state, we only consider magnetic fields increasing from zero up to the emergence of the Majorana state, while much greater values of Zeeman energies will not be of interest in this chapter. Technically, we truncate the spectrum to the set of 32 eigenvalues lying closer to zero energy. This truncation of the spectrum is imposing a superior limit for the energy such that the cross section is correctly computed. For higher energies our calculated cross section will always miss the transitions from states not included in our space. We shall discuss physical properties that do not depend on states lying much higher or much lower than zero. We are actually interested in the properties depending on the Majorana state lying very near zero energy.

Figure 3.3 shows the magnetic field dependence of the energy eigenvalues up to $\Delta_B = 0.5E_{so}$. The cross section is characterized by transitions among the system energy levels. For very small temperatures states at negative energies are occupied while states at positive energies are empty. For low values of $\Delta_B$ the energy spectrum is characterized by the presence of a wide gap centered on zero energy. This gap prevents any transition for energies lower than the corresponding energy jump ($\approx 0.5E_{so}$ in figure 3.3). When the Zeeman energy increases, the gap diminishes and eventually closes for $\Delta_B \approx 0.42E_{so}$ when the lowest energy levels collapse

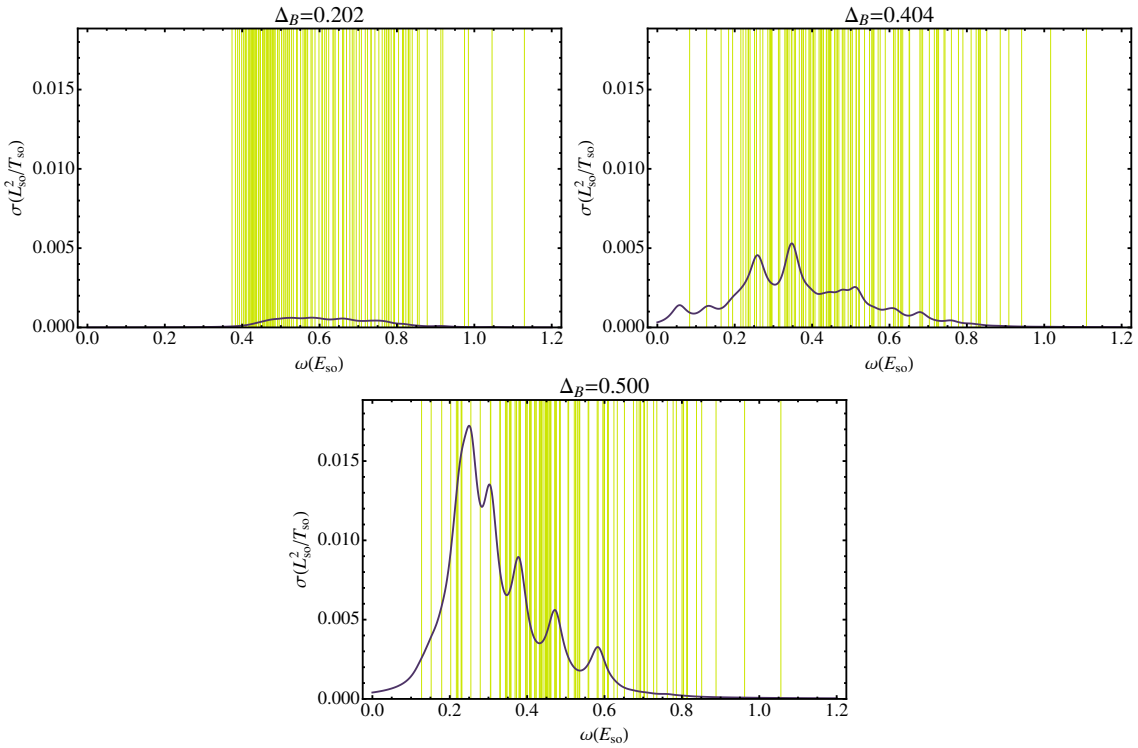


**Figure 3.4:** Three different representations of the cross section for different values of magnetic field. Thin vertical lines indicate the positions of all possible transitions from negative to positive energy levels, transitions from $-E$ to $E$ levels are neglected according with section 2.2. The calculations have been done with polarization along $\hat{x}$ and temperature $T = 0.045\,\mathrm{K}$.

into the Majorana state. In this configuration we may distinguish two types of transitions. The first group of transitions (type I) are those not involving the Majorana state and the second one (type II) are precisely the transitions from the Majorana state to the rest. The energy spectrum for $\Delta_B = 0.5E_{\mathrm{so}}$ shows again a gap smaller than the gap for vanishing Zeeman, with the Majorana state right in the middle.

Considering the optical transitions, the above scenario suggests the following criterion to infer the existence of a zero mode from experiments: if there is a transition in the cross section at energy lower than the gap then it must correspond to a transition from the mid-gap Majorana state. That is, in presence of a Majorana mode the lowest type II transition is at an energy which exactly equals half the energy of the lowest type I transition. Notice that the lowest transition of type I coincides with the gap in the spectrum (not counting the Majorana state). In the following we explicitly calculate the transition matrix elements to ascertain this scenario for different polarizations of the external field.

### Polarization along $\hat{x}$

We analyze first the cross section for polarization along $\hat{x}$, the long axis of the nanowire, for a low temperature ($T = 0.045$ K). In Fig. 3.4 we plot the computed cross sections for three selected Zeeman fields. Each panel also shows with thin vertical lines the positions of all possible transitions from negative to positive energy levels, moreover we have neglected all the lines

associated to transitions from energy levels $-E$ to the correspondent positive level $E$. We saw in section 2.2 that since the matrix element of the momentum operator is zero these no contribute to the cross section.
The first panel is for a low value of the Zeeman energy, when there is a clear gap, and we can see that the cross section although it is rather small concentrates as expected in an energy region with many transitions. In the second panel we can appreciate that the gap is very much reduced, as compared to the preceding panel, since transitions for lower energies are increasingly allowed. The reader should notice a peak, the first one in energy, without a corresponding vertical line. This is a temperature effect as can be deduced from the analysis of the data. Although the temperature is rather low, when the gap closes the first and the second negative energy levels become thermally activated and a transition between them can appear. For the third panel, as seen in Fig. 3.3, there is Majorana state. The manifestation in the cross section is not clear, since the lowest transition at $\omega \approx 0.12 E_{so}$ involving the Majorana state (type II) only creates a small bump on the cross section.

The dependence on magnetic field of the cross section can not be appreciated very well in figure 3.4. In figure 3.5 we have superposed in the same plot different cross sections to better see how this quantity changes. The cross section for low Zeeman energies is very small, almost flat compared with the results of high Zeeman energies. For low magnetic fields the cross section is near the cut off and this fact also induces a decrease of the cross section because we don't have the same contributions from the right hand side, when the Zeeman energy increases the main transitions go to the left and this effect is lower. Nevertheless, the effects of the cut off are not strong, we have enough eigenvalues to do the analysis. For $\Delta_B = 0.449 E_{so}$ we can see clearly that there are transitions for energies lower than the energy gap (the energy gap for type I transitions usually coincides with the highest peak of the cross section). In figure 3.6 we show the complete evolution of the cross section with Zeeman field as a three dimensional plot and as a contour plot. Although we can not extract very interesting conclusions from these figures they will be useful to compare with the results for polarization in $\hat{y}$ direction of the following section.

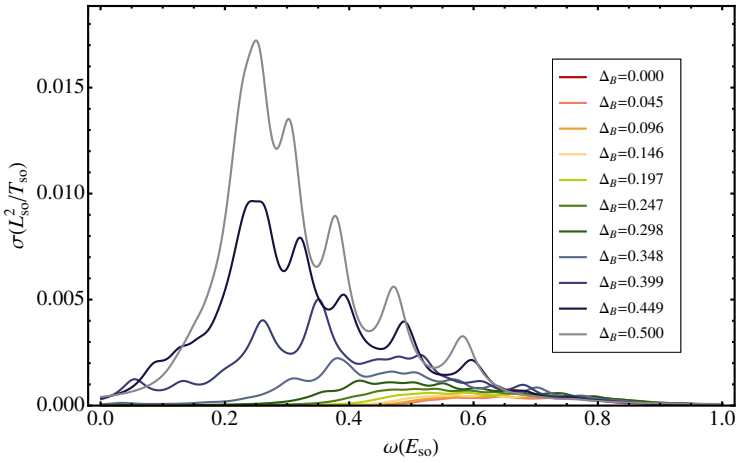


**Figure 3.5:** Different cuts at constant magnetic field of the cross section with polarization along $\hat{x}$ and temperature $T = 0.045\,\mathrm{K}$.

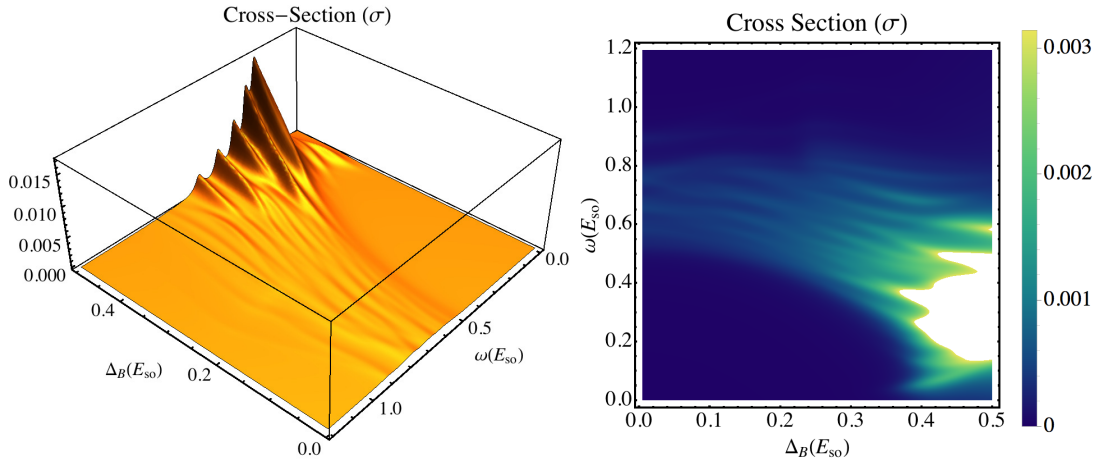


**Figure 3.6:** Magnetic field dependence of the cross section for $\hat{x}$ polarization and temperature $T = 0.045\,\mathrm{K}$. These representations show the complete evolution of the cross section, with the second panel focussing on the lower peaks of $\sigma$.

In figure 3.6 we see a general behavior that qualitatively resembles the eigenvalue distributions. As the magnetic field is increased there is a tendency to decrease the energy of the peaks, due to the gap closing. There is also a clear tendency to increase the height of the absorption peaks as the gap closes. The right panel shows the appearance of some subgap peaks of low intensity for $\Delta_B > 0.4E_{\mathrm{so}}$ but, as already mentioned, they are rapidly hidden by much higher peaks originating from transitions across the gap (type I).

### Polarization along $\hat{y}$

Contrary to the case of polarization along $\hat{x}$ of the preceding section, the manifestations of the presence of a Majorana state can be clearly seen with $\hat{y}$ polarization. Figure 3.7 shows these effects. In the first panel the presence of the gap forbids low energy transitions. Moreover, the cut off also introduces a decrease of the cross section. In the second panel the gap is almost closed and there are transitions at low energies. The lowest transition for this magnetic field achieve the maximum of the cross section, this can be also seen in figure 3.9 that show very clearly the evolution of the maximums. These four first maximums that appear in the second panel seems to follow some logarithmic or exponential decay, if we realize various fits the best is a quadratic one, however the results are not very good to affirm that follow some rule. The third panel corresponds to the configuration having the Majorana state, with a smaller gap, and it can be distinguished with the argument given above. The first transition is around $\omega \approx 0.12E_{so}$ while the gap for type I transitions is at $\omega \approx 0.25E_{so}$. This lower transition must involve the Majorana state. The remarkable thing is that with $\hat{y}$ polarization these low energy type II transitions are now strong enough to confirm the presence of a Majorana state. Furthermore, the cross section is such that the two groups of transitions can be clearly identified. The first group is, as we have said, the first group of transitions and the second one starts at the minimum that the cross section has in the middle, around $\omega \approx 0.25E_{so}$. We can see also in this third panel that around $\omega \approx 0.45E_{so}$ there is a dense group of transitions associated with the maximum, this is different from the case of $\hat{x}$ polarization, where this dense group is not the most contributing.

In figure 3.8 we superpose the cross sections for varying Zeeman energies in order to em-

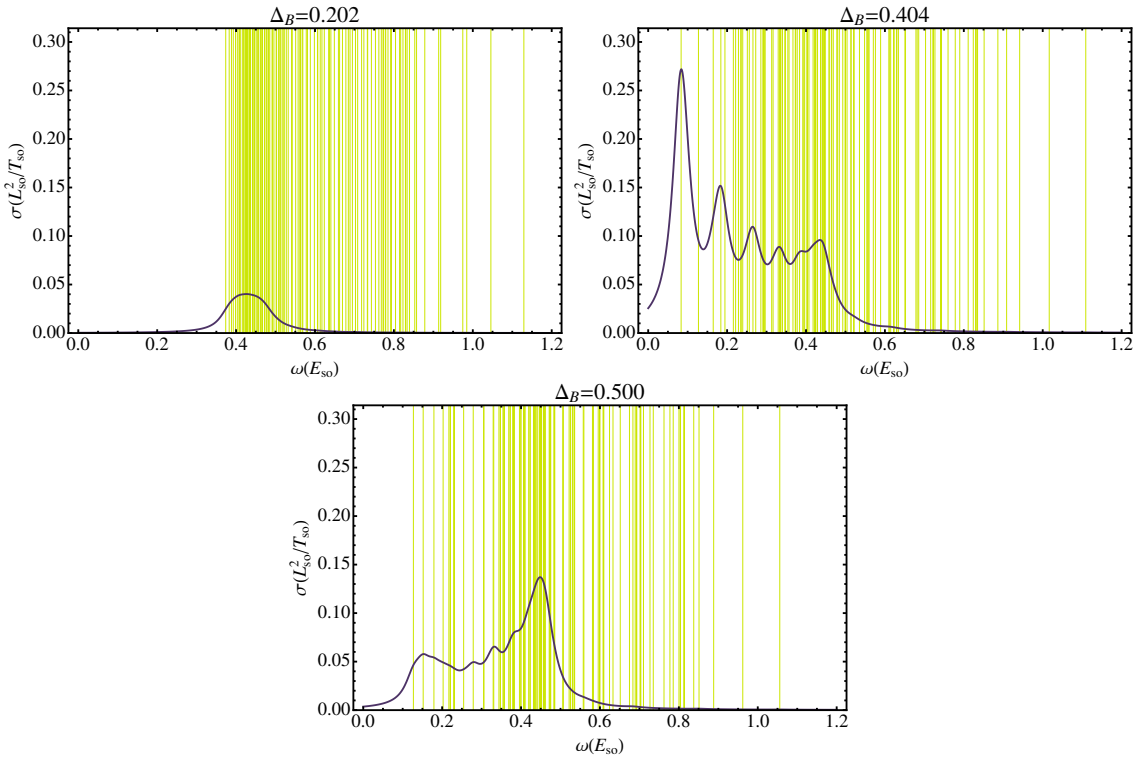


**Figure 3.7:** Three different representations of the cross section for different values of magnetic field with the possible transitions explained in section 3.2.1. Simulations with $\hat{y}$ polarization and temperature $T = 0.045\,\mathrm{K}$.

phasize the variation with the closing of the gap. Moreover we can see from this figure that there is no peak for energies higher than $\omega \approx 0.5E_{so}$, even though the set of eigenvalues contains transitions at such energies as shown by the vertical lines in 3.7. The interesting thing is this high-energy behaviour remains constant with magnetic field, contrary to the $\hat{x}$ polarization case. In figure 3.9 the phenomenon can be seen with more detail. We understand this as the combination of two effects: the first one is the finite number of eigenvalues in the analysis that, as explained above, gives a cut off in the cross section; the second one is the formation of subband grouping of the states in the finite system.

If we think in the energy solutions for the infinite square well $\varepsilon_n = \frac{\hbar^2\pi^2n^2}{2mL^2}$, for low values of $L$ the separation between levels is high, indicating that with strong confinement there is more separation between levels. A two dimensional system with strong confinement in the $y$ direction and lower confinement in the $x$ direction will have the levels organized in groups such that changing $n_x$ we change energy level within a group, while changing $n_y$ we change to another group of energy levels. Therefore when $n_y$ is changed the transition energy is higher than the corresponding change in $n_x$. The $\hat{x}$ polarization matrix elements involve $p_x$ and this operator changes the longitudinal mode of the wave function while, on the other hand, the $\hat{y}$ polarization involves matrix elements of $p_y$ and requires transitions that change the transversal modes. In conclusion, the $\hat{x}$ polarization cross section involves transitions within the same group while the $\hat{y}$ polarization induces transitions to a different group. From this point of view it is not a surprise that the truncation of the set of eigenvalues affects differently the $\hat{x}$ and $\hat{y}$ polarized cross sections.

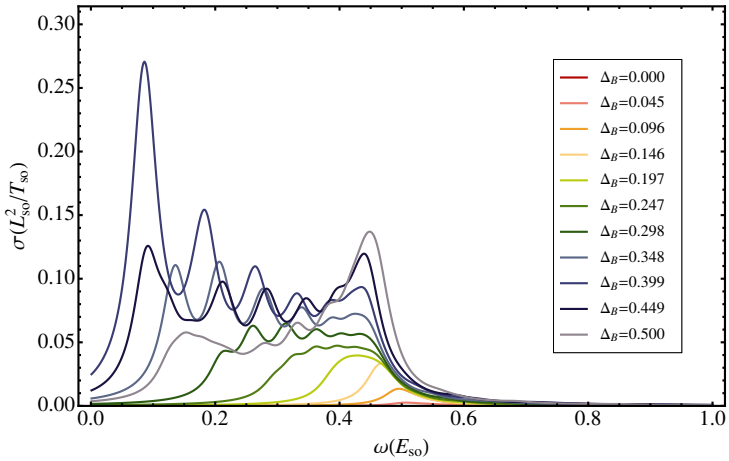


**Figure 3.8:** Different cuts at constant magnetic field of the cross section with polarization along $\hat{y}$ axis and temperature $T = 0.045K$.

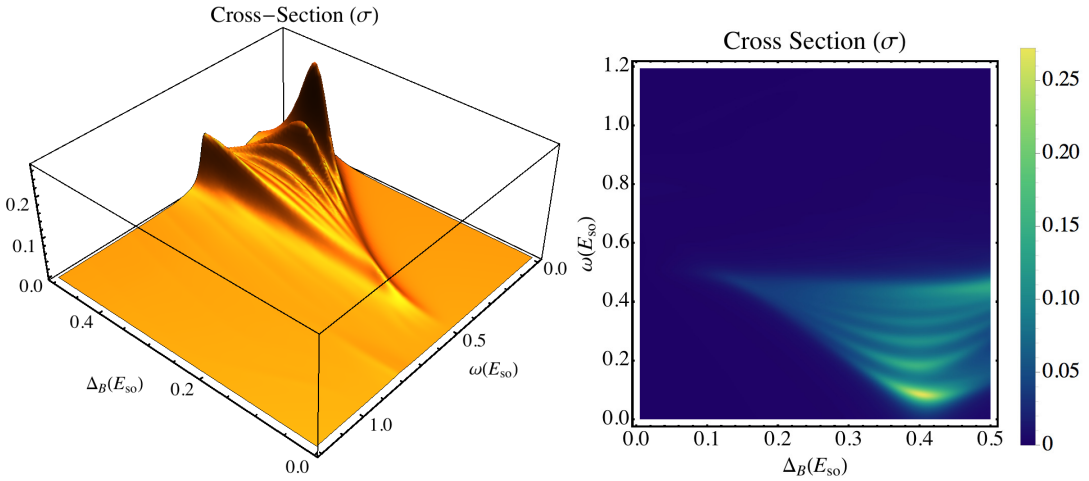


**Figure 3.9:** Magnetic field dependence of the cross section for $\hat{y}$ polarization and temperature $T = 0.045K$.

With the above interpretation in terms of subband groups we can understand somewhat better the results. We can interpret in figure 3.9 that the $\hat{y}$ polarization depends on transitions that change group and forbids lower transitions within the same group that make the spectrum less clear and hide the effect of the cut off.

### 3.2.2 Polarization effects

We present now the explicit dependence on polarization direction at constant magnetic field when the Majorana is well formed. In figure 3.10 we display the cross section for different values of the polarization angle $\varphi$ changing continuously from $\hat{x}$ to $\hat{y}$ direction. We have superposed the possible transitions in order to see which polarization activates which transition. The lowest curve, corresponding to $\hat{x}$ polarization is the same curve presented in the third panel of figure 3.4. The induced transitions by $\hat{y}$ start to grow when the polarization angle increases and

the $y$ component of the polarization vector becomes larger. Finally the induced transitions by $\hat{x}$ polarization fade away when the polarization angle $\varphi = 90°$. We can see clearly that the polarization along the $\hat{y}$ axis enhances the Majorana transitions (type II) that start at lower energies than the others.

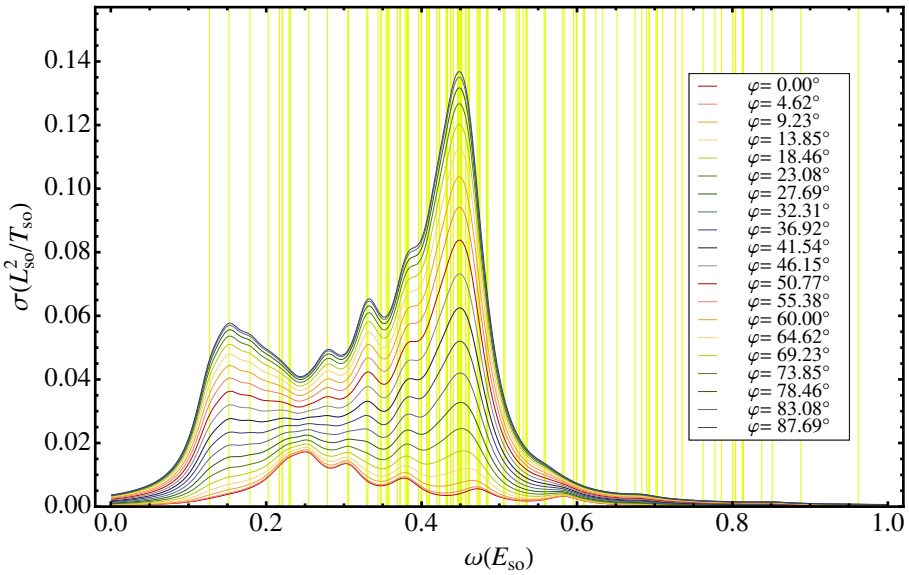


**Figure 3.10:** Cross section representations for different values of the polarization angle $\varphi$ (in degrees). The polarization angle changes from $\hat{x}$ polarization to $\hat{y}$ polarization. This simulations have been done at constant magnetic field $\Delta_B = 0.5E_{so}$ and temperature $T = 0.045K$.

One of the problems we should face in the experimental analysis of the absorption cross section is that we cannot distinguish if the spectrum starts at lower energies than the gap if we do not know the value of the gap. We suggest two ways to know the value of the gap: the first is using the theoretical prediction, the second is using the polarization effect. Since for polarization along $\hat{x}$ the spectrum starts at the energy of the gap we can extract the corresponding value from this experimental information. After that, we can change to polarization along $\hat{y}$ and, if lower transitions appear, we can infer the presence of a Majorana state.

### 3.2.3 Temperature effects

In the preceding subsections we have seen signatures in the spectrum of the presence of a Majorana state. However, we were considering a low temperature regime. For higher temperatures the thermal occupations start to play an important role in the transitions, with the possible transitions being not only restricted from negative energy to positive energy. We shall discuss the temperature dependence starting from low temperature $T = 0.045\,\mathrm{K}$ and increasing until $T = 4.523\,\mathrm{K}$ for the two extreme polarizations.

#### Thermal $\hat{x}$ polarization

In figure 3.11 we can see the temperature dependence for $\hat{x}$ polarization. In the upper panel we can see all the spectra while the lower one zooms in the lowest curves. For this polarization

the temperature effects are very strong with all the signatures of the low temperature cross section being washed out already for $T \approx 4$K. It is not a big surprise that quantum effects and temperature are not good friends. In the present case the situation becomes dramatic due to the large weight of the low energy transitions induced by the $p_x$ operator.

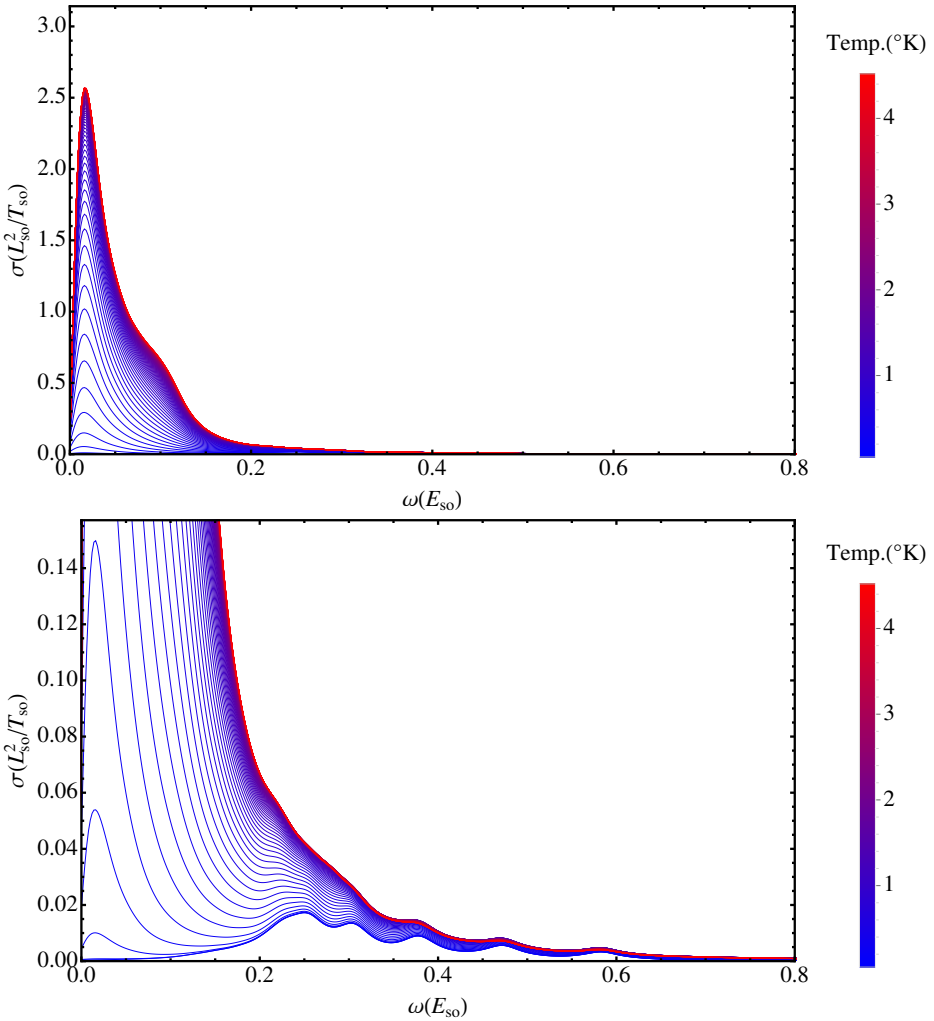


**Figure 3.11:** Evolution of the cross section as a function of temperature for polarization along $\hat{x}$ and constant magnetic field $\Delta_B = 0.5E_{so}$. Different curves of the cross section are presented, the temperature of each one being determined by the color according to the legend. The first panel shows all the curves while the second one zooms in the low temperature part.

### Thermal $\hat{y}$ polarization

A qualitatively different behavior is seen for the $\hat{y}$ polarization. When the temperature increases in the same interval as before some low energy transitions appear, but the good thing is that these transitions do not cover the low temperature features of the cross section. The intensity of the transitions diminishes with temperature but the Majorana transitions remain clearly visible. This protection is again due to the $\hat{y}$ polarization not allowing low energy transitions within the same group of states. We believe this is an important result, suggesting the manifestation

of a Majorana state at relatively high temperatures. For a nanostructure four kelvins is a considerable temperature, and the Majorana transitions remain there. This fact could be an important argument to use spectroscopy with the aim of detecting Majorana states.

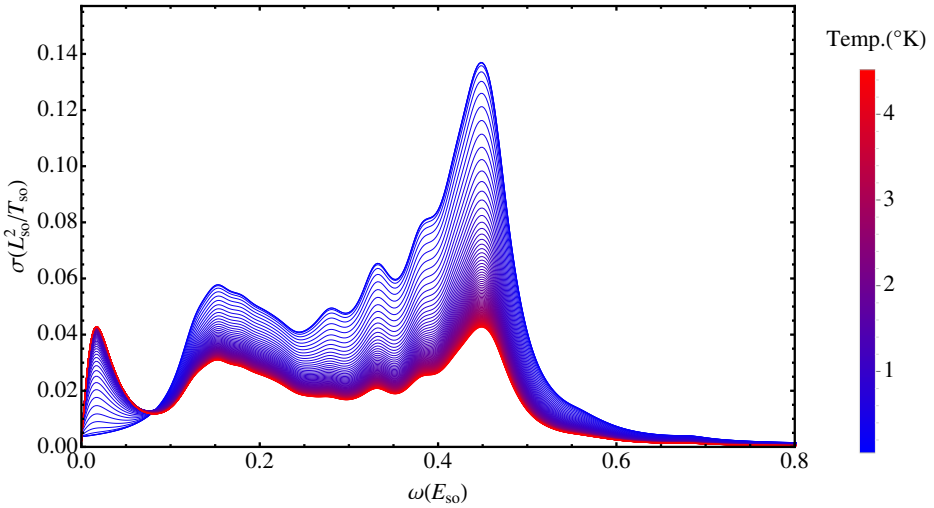


**Figure 3.12:** Evolution of the cross section as a function of temperature for polarization along $\hat{y}$ and constant magnetic field $\Delta_B = 0.5E_{so}$. Different curves of the cross section are presented, the temperature of each one is determined by the color according with the legend.

# Conclusions

The main aim of this work is the study of Majorana states in order to understand better the interesting properties that they manifest. More specifically, the understanding of those properties that could help to detect these peculiar states in experiment. In the first pages of this work we argued the connections with Particle Physics and the possible applications in Quantum Computation. The detection and manipulation of Majorana states is an important aim for science, and of course a good topic to devote our efforts.

We have studied in this work more specifically the optical properties but we have also reviewed in a more general way the properties of the Majorana states described by the Bogoliubov-deGennes hamiltonian. One of the things that we have seen are the conditions that must fulfill a system to host Majorana states. We have also seen the implications of the symmetries of the Bogoliubov-deGennes hamiltonian on the optical spectrum, forbidding transitions from energy levels $-E$ to the correspondent positive ones $E$. Furthermore, we have classified the transitions in two types, whether or not involving the Majorana state.

Referring to the optical properties of the system, we have analyzed the dependence on different parameters. One of the important things in this part is the energy gap and how it changes with the Zeeman energy. The gap is vital to detect Majorana states. The polarization effect points out the differences in the inference of Majoranas, while polarization along the $\hat{x}$ axis does not show very well the presence of a Majorana state, polarization along $\hat{y}$ axis very clearly manifests the presence of this. Moreover, polarization along $\hat{y}$ axis also evidences larger energy transitions for the transversal mode of the wave function. Polarization effects give us a useful method to determine experimentally the energy gap. The gap can be measured using $\hat{x}$ polarization and this may help to infer the presence of the Majorana state for polarization along $\hat{y}$ axis. Finally, the dependence with temperature also shows a strong difference between the two polarizations. In the case of $\hat{x}$ polarization the temperature effects rapidly destroy all the signatures of the initial spectrum, while the $\hat{y}$ polarization shows a strong resistance. This resistance is due to the higher energy transitions in $\hat{y}$ polarization, better avoiding the thermal smearing of the gap.

To sum up, the analysis presented in this work can help to understand in a better way the properties of the Majorana states. Our results can motivate the use of novel techniques like optical spectroscopy that could be useful to detect the Majorana states and confirm their existence in nanowires.

# Bibliography


[1] E. Majorana, "Teoria simmetrica dell'elettrone e del positrone," *Nuovo Cimento*, vol. 14, pp. 171–184, 1937.

[2] B. Martin and G. Shaw, *Particle physics*. John Wiley & Sons, 2008, vol. 45.

[3] W. B. Rolnick, *The fundamental particles and their interactions*. Addison-Wesley, 1994.

[4] G. Danby, J. Gaillard, K. Goulianos, L. Lederman, N. Mistry, M. Schwartz, and J. Steinberger, "Observation of high-energy neutrino reactions and the existence of two kinds of neutrinos," *Physical Review Letters*, vol. 9, no. 1, pp. 36–44, 1962.

[5] C. Nayak, S. H. Simon, A. Stern, M. Freedman, and S. Das Sarma, "Non-abelian anyons and topological quantum computation," *Reviews of Modern Physics*, vol. 80, p. 1083, 2008.

[6] J. Alicea, "New directions in the pursuit of majorana fermions in solid state systems," *Reports on Progress in Physics*, vol. 75, p. 076501, 2012.

[7] C. Beenakker, "Search for majorana fermions in superconductors," *Annual Review of Condensed Matter Physics*, vol. 4, no. 1, pp. 113–136, 2013.

[8] M. Franz, "Majorana's wires," *Nature Nanotechnology*, vol. 8, no. 3, pp. 149–152, 2013.

[9] T. D. Stanescu and S. Tewari, "Majorana fermions in semiconductor nanowires: fundamentals, modeling, and experiment," *Journal of Physics: Condensed Matter*, vol. 25, no. 23, p. 233201, 2013.

[10] V. Mourik, K. Zuo, S. Frolov, S. Plissard, E. Bakkers, and L. Kouwenhoven, "Signatures of majorana fermions in hybrid superconductor-semiconductor nanowire devices," *Science*, vol. 336, pp. 1003–1007, 2012.

[11] M. T. Deng, C. L. Yu, G. Y. Huang, M. Larsson, P. Caroff, and H. Q. Xu, "Anomalous zero-bias conductance peak in a Nb-InSb nanowire-Nb hybrid device," *Nano Letters*, vol. 12, no. 12, pp. 6414–6419, 2012.

[12] L. P. Rokhinson, X. Liu, and J. K. Furdyna, "The fractional ac josephson effect in a semiconductor-superconductor nanowire as a signature of majorana particles," *Nature Physics*, vol. 8, no. 11, pp. 795–799, 2012.

[13] A. Das, Y. Ronen, Y. Most, Y. Oreg, M. Heiblum, and H. Shtrikman, "Zero-bias peaks and splitting in an Al-InAs nanowire topological superconductor as a signature of majorana fermions," *Nature Physics*, vol. 8, no. 12, pp. 887–895, 2012.

[14] A. D. K. Finck, D. J. Van Harlingen, P. K. Mohseni, K. Jung, and X. Li, "Anomalous modulation of a zero-bias peak in a hybrid nanowire-superconductor device," *Physical Review Letters*, vol. 110, p. 126406, 2013.

[15] Y. Oreg, G. Refael, and F. von Oppen, "Helical liquids and majorana bound states in quantum wires," *Physical Review Letters*, vol. 105, p. 177002, 2010.

[16] L. Serra, "Majorana modes and complex band structure of quantum wires," *Physical Review B*, vol. 87, p. 075440, 2013.

[17] J. Klinovaja and D. Loss, "Composite majorana fermion wave functions in nanowires," *Physical Review B*, vol. 86, p. 085408, 2012.

[18] J. Osca, D. Ruiz, and L. Serra, "Effects of tilting the magnetic field in one-dimensional majorana nanowires," *Physical Review B*, vol. 89, no. 24, p. 245405, 2014.

[19] HSL (2013). A collection of Fortran codes for large scale scientific computation. http://www.hsl.rl.ac.uk".

[20] E. Merzbacher, *Quantum mechanics*. New York: Wiley, 1998.

[21] U. Merkt, "Far-infrared spectroscopy of quantum dots," *Physica B: Condensed Matter*, vol. 189, no. 1, pp. 165–175, 1993.

[22] J. Phillips, K. Kamath, and P. Bhattacharya, "Far-infrared photoconductivity in self-organized InAs quantum dots," *Applied Physics Letters*, vol. 72, no. 16, pp. 2020–2022, 1998.

[23] T. Demel, D. Heitmann, P. Grambow, and K. Ploog, "Far-infrared response of one-dimensional electronic systems in single- and two-layered quantum wires," *Physical Review B*, vol. 38, no. 17, p. 12732, 1988.

[24] V. Gudmundsson, A. Brataas, P. Grambow, B. Meurer, T. Kurth, and D. Heitmann, "Bernstein modes in quantum wires and dots," *Physical Review B*, vol. 51, no. 24, p. 17744, 1995.

[25] C. Steinebach, D. Heitmann, and V. Gudmundsson, "Far-infrared absorption of acoustic and optical magnetoplasmons in double-layered quantum wires," *Physical Review B*, vol. 56, no. 11, p. 6742, 1997.

[26] T. Demel, D. Heitmann, P. Grambow, and K. Ploog, "One-dimensional plasmons in AlGaAs/GaAs quantum wires," *Physical Review Letters*, vol. 66, pp. 2657–2660, 1991.

[27] P. L. Richards, "High-resolution fourier transform spectroscopy in the far-infrared," *Journal of the Optical Society of America*, vol. 54, no. 12, pp. 1474–1484, 1964.